J Mol Model (2008) 14:1131–1145
DOI 10.1007/s00894-008-0356-2

ORIGINAL PAPER

Exploring the binding features of rimonabant analogues and acyclic CB_1 antagonists: docking studies and QSAR analysis

Elena Cichero · Giulia Menozzi · Andrea Spallarossa · Luisa Mosti · Paola Fossa

Received: 7 April 2008 / Accepted: 15 July 2008 / Published online: 12 August 2008

Abstract In order to elucidate the structural requirements for human CB_1 receptor antagonism, 78 antagonists belonging to five different chemical classes were selected from the literature and docked into the receptor binding site, built by homology modeling techniques. To further explore the structure-activity relationships within the considered chemical classes, a pharmacophore model and a QSAR analysis were developed. In a first step five alignments, one for each group of compounds were generated. All of them were then submitted to a MOE pharmacophore search in order to obtain a final pharmacophore model representative of the whole dataset which was used to elaborate the following 3D-QSAR analysis, by means of the CoMFA methodology. The results of these investigations are expected to be useful in the process of design and development of new potent CB_1 antagonists.

Keywords CB_1 receptor antagonists · CoMFA · Docking · 3D-QSAR

Introduction

The recent discovery of the endogenous cannabinoid system (ECS) comprising the cannabinoid receptors (namely, CB_1 and CB_2) [1], endogenous ligands, and enzymes for ligands metabolism has fostered new targeted studies into the therapeutic potential of human CB_1 and CB_2 receptors agonists and antagonists. A number of pharmacological studies have shown that CB_1 agonists can be potentially useful in the treatment of nausea, glaucoma, cancer, stroke, pain, immune suppression and neuronal disorders such as multiple sclerosis and Parkinson's disease [2, 3] whereas CB_1 antagonism could be involved in the management of obesity, detoxification from drug abuse or nicotine dependence, and, more in general, in the regulation of different relapsing phenomena [4].

Rimonabant (SR141716, Acomplia) is a 1,5-diaryl pyrazole derivative which represents the prototype of the selective human CB_1 antagonist to date. Molecular variations of rimonabant pyrazole substituents and nucleus led to a number of (poly)cyclic and linear derivatives, as described in the literature [5–10]. With the aim at identifying the structural basis for human CB_1 receptor antagonism and the molecular properties able to modulate the affinity for the receptor, a dataset of 78 CB_1 antagonists showing different scaffolds (i.e. pyrazoles, tetrahydropyrrolo-pyridines, 1,4-dihydroindeno[1,2-*c*]pyrazoles, pyrazolo-pyrimidines and acyclic sulphonamide derivatives) has been selected form literature and submitted to a docking study. In order to overcome the limitations derived from the absence of a reliable X ray target structure, in tandem with a homology modelling based procedure, a ligand-based molecular modelling tool has been applied. Thus, we generated common features pharmacophore hypothesis in order to identify the most relevant chemical requirements for receptor antagonism. Furthermore, quantitative structure–activity relationships (QSAR) studies were performed on the same compound set to derive more complete guidelines for the synthesis of new compounds.

E. Cichero · G. Menozzi · A. Spallarossa · L. Mosti · P. Fossa (✉)
Dipartimento di Scienze Farmaceutiche,
Università degli Studi di Genova,
Viale Benedetto XV n.3,
16132 Genova, Italy
e-mail: fossap@unige.it

Materials and methods

Data set

The molecular structures of **1**–**78** (Table 1) were built, parameterized (Gasteiger-Huckel method) and energy minimized within MOE using MMFF94 force field [11]. In order to ensure comparable values for biological activity, only compounds screened by the same pharmacological protocol (binding affinity derived from inhibition of binding of [3H]CP-55940 to recombinant human CB1 receptors expressed on Chinese hamster ovary cells) were included in the set. The enzyme inhibitory activity of all molecules covered 5 log orders. For QSAR analysis, K_i values have been transformed into pK_i, and then used as the response variable. Compounds **1**–**78** were grouped into five groups, according to their chemical structures and Gasteiger Huckel atomic charges were calculated. Then they were

Table 1 Molecular formulas of compounds **1**–**78**

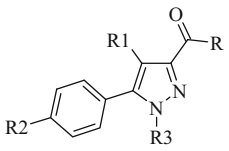

Group 1

Compound	R	R1	R2	R3	pKi	Ref.
1, Rimonabant	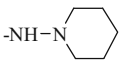	$-CH_3$	Cl	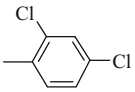	7.9	5
2	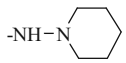	H	H	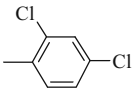	6.7	5
3	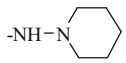	H	Cl	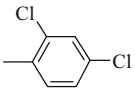	7.4	5
4		$-CH_3$	Cl	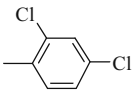	7.9	6
5	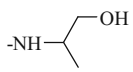	$-CH_3$	Cl	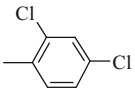	6.9	6
6	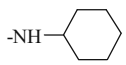	$-CH_3$	Cl	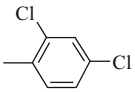	8.9	6
7	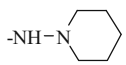	$-CH_3$	Br	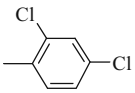	7.8	5
8	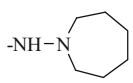	$-CH_3$	Br	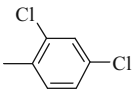	8.1	5
9	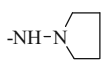	$-CH_3$	Br	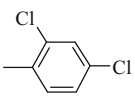	7.8	5

Table 1 (continued)

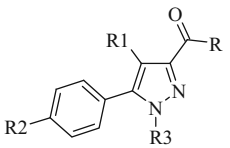

Group 1

Compound	R	R1	R2	R3	pKi	Ref.
10	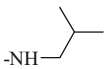	$-CH_3$	Cl	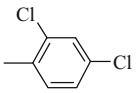	8.0	6
11		$-CH_3$	Cl	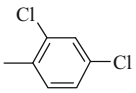	7.3	5
12	$-NH(CH_2)_3OH$	$-CH_3$	Cl	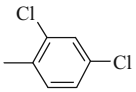	6.8	5
13	$-NH(CH_2)_2OH$	$-CH_3$	Cl	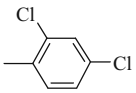	6.4	6
14	$-NHNH_2$	$-CH_3$	Cl	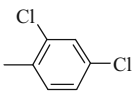	6.2	5
15	$-NH-NHCH_2CH_3$	$-CH_3$	Cl	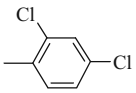	6.8	5
16	$-NH-NHCH_2CH_2CH_3$	$-CH_3$	Cl	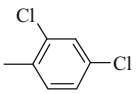	7.2	6
17	$-NH-NH(CH_2)_3CH_3$	$-CH_3$	Cl	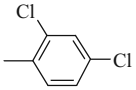	7.4	6
18	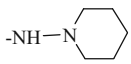	$-CH_3$	Cl		7.2	5

manually divided into a training set (**1–6, 8–13, 15–23, 25–31, 33–44, 46–57, 59–61, 63–69, 71–78**) and a test set (**7, 14, 24, 32, 45, 58, 62, 70**) in such a way that, for each group, both the training and the test sets contained a representative range of biological activities and structural variations.

Docking studies

A 3-D model of the human CB_1 receptor was built by means of homology modelling techniques, starting from the three-dimensional structure co-ordinate file of bovine rhodopsin (PDB entry 1F88) according to the procedure described by us in [12]. Each antagonist was docked into the putative binding site of the CB_1 receptor using the flexible docking module implemented in MOE. For all compounds the best-docked geometries, evaluated in terms of "Affinity dG" (kcal mol^{-1} of total estimated binding energy), were employed in order to identify the most probable ligand bioactive conformation.

Pharmacophore search

Even though a structure-based approach is possible with CB_1 receptor model built by homology modelling techni-

Table 1 (continued)

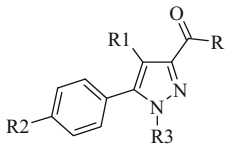

Group 1

Compound	R	R1	R2	R3	pKi	Ref.
19	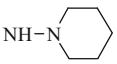	H	H	$-(CH_2)_6CH_3$	6.5	5
20	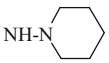	CH_3	H	$-(CH_2)_6CH_3$	6.7	5
21	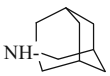	$-CH_3$	H	$-(CH)_5F$	8.9	5
22	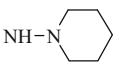	$-CH_3$	H		6.2	5
23	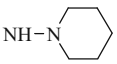	$-CH_3$	Br	$-(CH_2)_4CH_3$	7.1	5
24	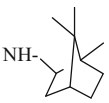	$-CH_3$	Br	$-(CH)_5Cl$	8.3	5

ques, a ligand based approach like pharmacophore analysis followed by CoMFA studies [13, 14] may provide a complementary tool for drug design.

Starting from the best geometries obtained by conformational analysis, five alignments were derived, one for each chemical group of compounds (Table 1) using the MOE pharmacophore search module, setting tolerance to 1.20 and threshold to 98%. Only those features showing a score > 90% were retained for each alignment. Subsequently, the five pharmacophoric hypothesis were merged together and their common features, identified in the first step, were used as reference points for superimposing all compounds.

Thus, on the base of these requirements, a final alignment was obtained for the following CoMFA calculations.

3D-QSAR analysis

CoMFA procedure

CoMFA method is a widely used 3D-QSAR technique to relate the biological activity of a series of molecules with their steric and electrostatic fields which are calculated placing the aligned molecules, one by one, in a 3D cubic lattice with 2 Å grid spacing. The column-filtering threshold value in this study was set to 2.0 kcal mol^{-1}, to improve the signal-noise ratio. A methyl probe with a + 1 charge is used to calculate steric and electrostatic fields, represented by van der Waals potential and columbic term, respectively. A 30 kcal mol^{-1} energy cut-off was applied to avoid infinity of energy values inside the molecule.

Table 1 (continued)

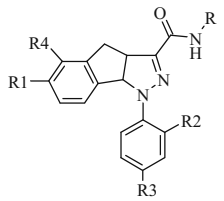

Group 2

Compound	R	R1	R2	R3	R4	pKi	Ref.
25	$-NH_2$	Cl	Cl	Cl	H	5.7	7
26	$-N(CH_3)_2$	Cl	Cl	Cl	H	5.7	7
27		Cl	Cl	Cl	H	5.5	7
28		Cl	Cl	Cl	H	6.1	7
29		Br	Cl	Cl	H	5.8	7
30		$-CH_3$	Cl	Cl	H	6.4	7
31		Cl	H	Cl	H	5.7	7
32		F	Cl	Cl	H	5.9	7
33		$-OCH_3$	Cl	Cl	H	6.4	7
34		H	Cl	Cl	Cl	6.1	7
35		H	Cl	Cl	H	5.9	7
36		Cl	Cl	Cl	H	5.7	7
37		Cl	H	$-OCH_3$	H	5.5	7
38		Cl	H	H	H	5.3	7
39		I	Cl	Cl	H	6.5	7

Regression analyses were performed applying the partial least squares (PLS) algorithm in Sybyl; the steric field alone and the combination of the steric and electrostatic fields were used as structural descriptors to evaluate their correlation with the inhibitory activity (expressed as pK_i) data. PLS with cross-validation, performed using ten cancellation groups was used to identify the optimal number of components to be used in the subsequent analyses. The final CoMFA model was generated using non-cross-validated PLS analysis. To further assess the statistical confidence and robustness of derived model, a 100-cycle bootstrap analysis was performed.

Conformational analysis, docking studies and the alignment procedure were performed using the Molecular Operating Environment (MOE; version 2008.08) suite. CoMFA was performed using Sybyl (Tripos, version 7.2) [14]. All calculations were carried out using a PC, with operative system windows XP and an SGI O2 Silicon Graphics.

Table 1 (continued)

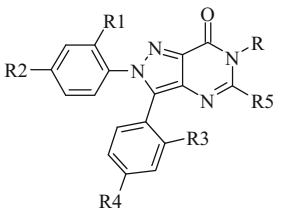

Group 3

Compound	R	R_1	R_2	R_3	R_4	R_5	pKi	Ref.
40		H	Cl	Cl	H	H	7.4	8
41		Cl	H	H	Cl	H	7.7	8
42	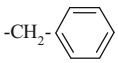	Cl	H	H	Cl	H	8.3	8
43		Cl	H	H	Cl	H	7.9	8
44	$-CH_2CF_3$	H	Cl	Cl	H	H	7.5	8
45	$-CH_2CF_3$	Cl	H	H	Cl	H	8	8
46	$-CH_2CF_3$	Cl	H	H	Cl	$-CH_2CH_3$	8	8
47		Cl	H	H	Cl	H	7.6	8

Results and discussion

Docking poses

According to docking studies carried out on rimonabant and other CB_1 antagonists [15, 16], three different receptor sub cavities (namely P1, P2 and P3) would be involved in receptor-ligand interaction. In particular, P1 (formed by Lys192, Thr197 and Ser383) is an hydrogen bond site deemed to be crucial for the receptor antagonism; P2 hosts residues (e.g. Phe174, Phe177, Val196, Ala380, Met384 and Leu387) capable of Van der Waals interaction with the ligand; P3 (formed by Phe200, Tyr275, Trp279, Trp356, Met363 and Phe379) is an hydrophobic region where π–π stacking or Van der Waals interactions can occur.

Docking poses calculated for antagonists **1**–**78** are consistent with the occupation of P1-P3 sub cavities and structurally rationalize the differences in hCB$_1$ binding affinities as detailed below.

Group 1, Compounds 1–24

Group 1 compounds and rimonabant display similar binding poses with the R substituent located in the P2 sub cavity and R2-R3 substituents inserted in P3 (Fig. 1).

Interestingly, the most active compounds (**6–10**) establish two hydrogen bonds with the ε amino group of Lys192 (P1 region), involving the first the oxygen atom of the carbonylic group in position 3 and the second the nitrogen atom of the amide/hydrazide function in position 3.

Table 1 (continued)

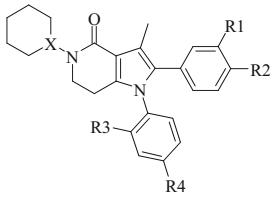

Group 4

Compound	X	R1	R2	R3	R4	pKi	Ref.
48	CH	H	$-CH_3$	Cl	Cl	8.0	9
49	CH	H	F	Cl	Cl	8.2	9
50	CH	$-OCH_3$	$-OCH_3$	Cl	Cl	8.2	9
51	CH	H	$-OCH_3$	Cl	Cl	8.1	9
52	CH	H	$-CF_3$	Cl	Cl	8.4	9
53	CH	H	$-CH$	Cl	Cl	8.0	9
54	CH	$-CH_3$	H	Cl	Cl	7.8	9
55	CH	$-OCH_3$	H	Cl	Cl	8.2	9
56	CH	H	H	Cl	Cl	7.8	9
57	CH	H	Cl	Cl	Cl	8.1	9
58	CH	H	Cl	Cl	H	8.5	9
59	N	H	Cl	Cl	Cl	8.7	9
60	N	H	Cl	Cl	H	8.5	9
61	CH	H	$-OCH_3$	Cl	H	8.1	9
62	N	H	$-OCH_3$	Cl	H	7.7	9
63	CH	H	F	$-CH_3$	H	7.4	9
64	CH	H	$-OCH_3$	$-CH_3$	H	7.7	9
65	N	H	$-OCH_3$	$-CH_3$	H	7.1	9

Group 2, Compounds 25–39

25–39, being bulkier than their pyrazole analogues, are not able to properly occupy the P1 and P2 binding pockets and show only a hydrogen bond between the carbonylic oxygen at position 3 and the ε amino group of Lys192. This observation could rationalize the decrease in binding affinity for these compounds in comparison with rimonabant analogues (group 1) (Fig. 2a). The aromatic portions of these ligands display the same hydrophobic interactions of rimonabant phenyl rings within the P3 pocket.

Group 3, Compounds 40–47

In compounds **40–47**, the amidic function at position 3 (1,5 diaryl pyrazole derivatives numbering) is incorporated in a pyrazolopyrimidinone scaffold with a reduction of the conformational flexibility. The most active compounds of this series (**42**, **45**, **46**, pKi greater than 8) are hydrogen bonded to Lys192 and to Thr197 that contact the carbonyl oxygen and the pyrazole nitrogen at position 2, respectively. Aromatic rings are properly located into P3 pocket, performing π–π interactions with hydrophobic residues Tyr275, Trp279 and Trp 356 (Fig. 2b).

Table 1 (continued)

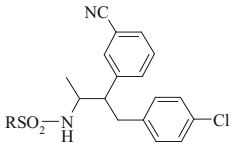

Group 6

Compound	R	pKi	Ref.	Compound	R	pKi	Ref.
66	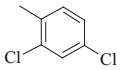	8.1	10	**72**	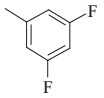	8.3	10
67		8.0	10	**73**	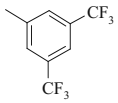	8.5	10
68	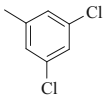	7.9	10	**74**	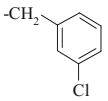	7.3	10
69	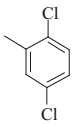	8.1	10	**75**	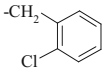	7.8	10
70		7.5	10	**76**	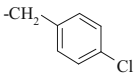	7.8	10
71	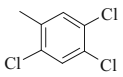	7.8	10	**77**	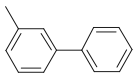	8.6	10
				78	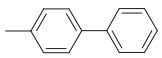	7.6	10

All pKi values are referred to S,S diasteroisomers

Group 4, Compounds 48–65

46–**65** are characterized by high pKi values and all display two hydrogen bonds with the receptor binding site. The first one is formed between the pyridonic nitrogen atom and the ε amino group of Lys192; the second is established between the carbonylic oxygen and the hydroxyl group of Ser383 side chain. As above noted, the aromatic rings are properly located in P3 pocket performing π–π stacking interactions with Tyr275, Trp279 and Trp 356 (Fig. 2c).

Group 5, Compounds 66–78

According to the calculated binding mode, **66**–**78** share the following interactions with the human CB_1 receptor: i) a hydrogen bond between the Lys192 ε amino group and the oxygen of the sulphonic moiety; ii) a H-bond between the second oxygen of the sulphonic moiety and the OH group of Ser383, iii) cation-π interactions between the Lys192 ε amino group and R substituent Ph portion (Fig. 2d).

According to our docking calculations, all the compounds display the same common interactions: i) a single or double hydrogen bond with the ε amino group of Lys192, ii) one or more π–π stackings with aromatic residues Tyr275, Trp279, Trp356 and Phe379. These amino acids appear to be key residues for the CB_1 antagonism. However, up to date, only the importance of the interaction with Lys 192 has been highlighted by site-directed mutagenesis experiments. Comparing the binding modes of groups 1–5, we can conclude that the replacement of the pyrazole ring with a bicyclic one or with a linear moiety (see groups 3–6) increase the binding affinities for those compounds which are able to display additional interactions. Among these, the most recurring are: i) an additional hydrogen bond with Thr197 (group 3) or with Ser383 (groups 4–5), ii) a second hydrogen bond with Lys192 (group 5), iii) a cation-π interaction between Lys192 ε

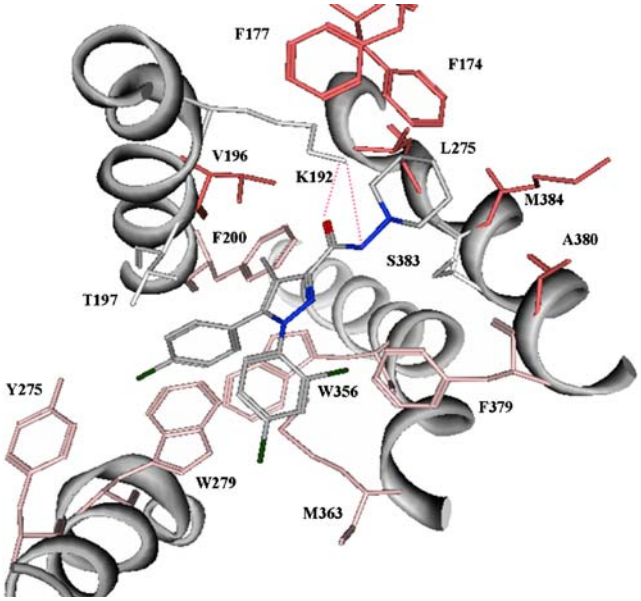

Fig. 1 Docking pose of rimonabant, **1** (stick, coloured by atom type, C atoms in grey) into the CB_1 receptor binding site. P1, P2 and P3 pockets residues are reported respectively in white, dark pink and pink sticks. The most important residues are labelled, hydrogen bonds are coloured in pink

amino group and an aromatic portion of the molecule (group 5).

On the contrary, compounds **25**–**39** (group 2) which display only a single hydrogen bond interaction with Lys192, do not present an optimal binding affinity. In addition, they do not properly occupy P1 and P2 pockets.

Pharmacophore search

Five different pharmacophore searches were developed in order to highlight the most important key features showed by each group of compounds belonging to the dataset (Figs. 3, 4, 5, 6 and 7). All of them share the following requirements: two hydrophobic-aromatic features (HY1 and HY2) and one hydrogen bond acceptor function (HA). For all the compounds, these three pharmacophoric elements are spatially oriented so as to form a triangle were the distance between HY1 and HY2 ranges from 4.70 to 5.45 Å (mean value 4.94 Å); the distance between HY1 and HA ranges from 5.75 to 6.90 Å (mean value 6.49 Å); the distance between HY2 and HA ranges from 6.20 to 7.57 Å (mean value 7.14 Å).

This triangular disposition of the three pharmacophoric elements suggests the importance of a specific Y shape the CB_1 antagonist should assume into the receptor binding site.

The pharmacophore hypothesis is in good agreement with the homology modelling structure-based studies. In fact, in the final pharmacophore model, for all compounds the hydrogen bond acceptor (HA) feature identifies that portion of the ligand which docking studies describe as involved in a H-bond with Lys192 ε amino group. Moreover, the hydrophobic or π–π stacking interactions between ligands and receptor equally play a crucial role, in fact the other two pharmacophore features of our map have hydrophobic nature (Fig. 8). These three common features were used to align compounds **1**–**78** prior to develop the CoMFA analysis.

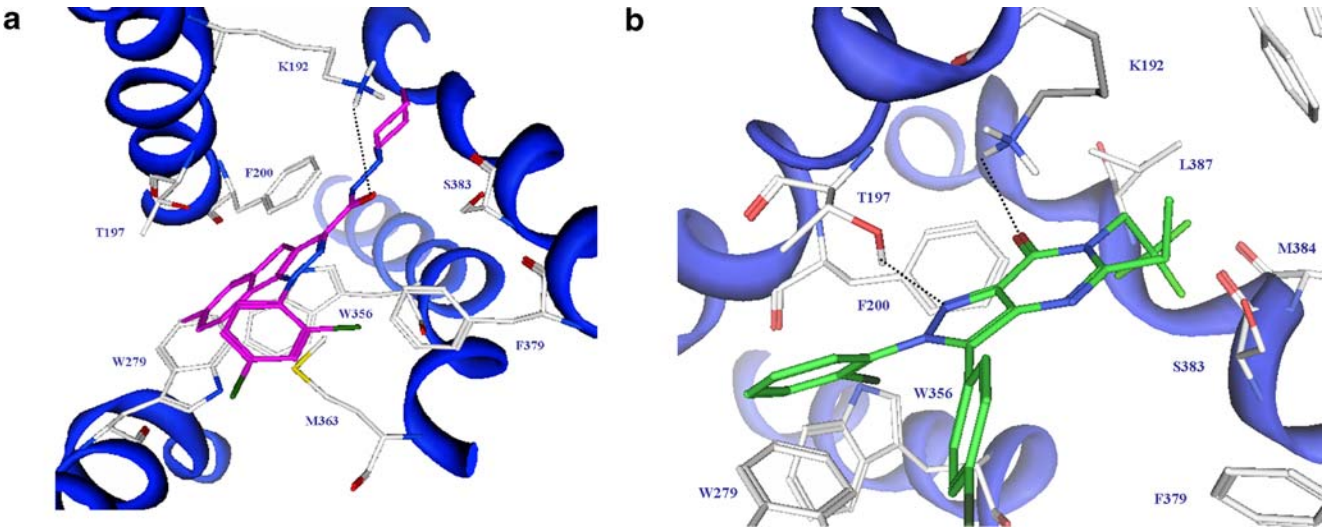

Fig. 2 Docking analysis into hCB_1 receptor model: (**a**) docking pose of **30** (stick model, colour code: C, magenta; N, blue; O, red; Cl, green); (**b**) docking pose of **46** (stick, colour code: C, green; N, blue; O, red; Cl, green), (**c**) docking pose of **48** (stick, C carbon: gold); (**d**) docking pose of **77** (C carbon: pink). The most important residues are labelled, hydrogen bonds are coloured in black

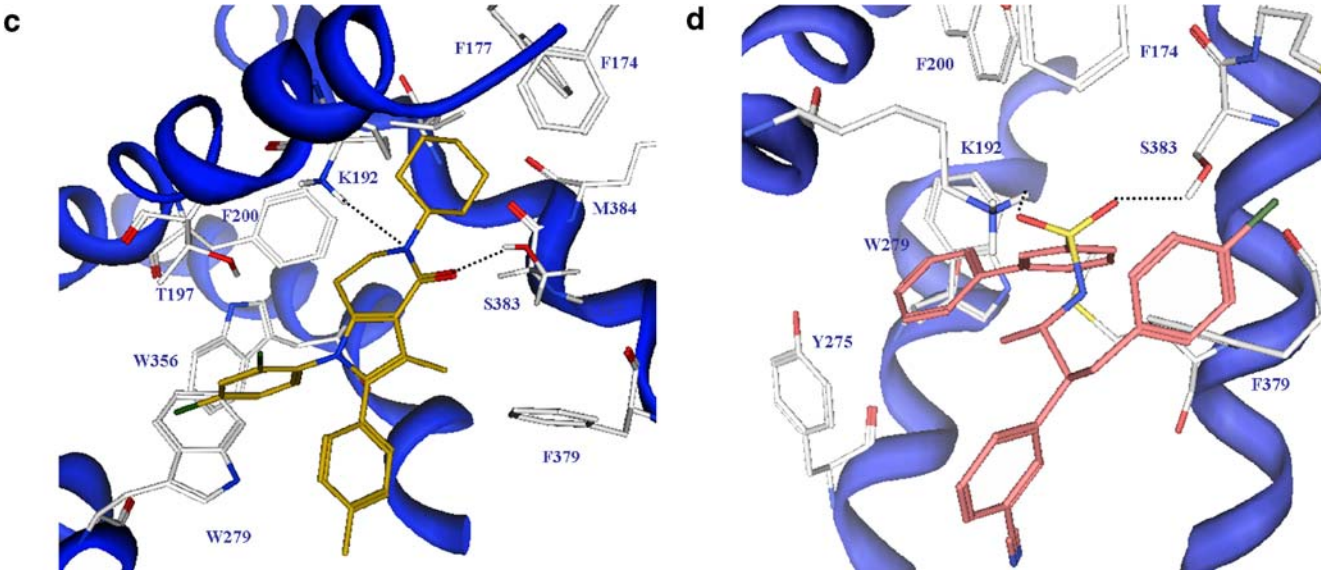

Fig. 2 (continued)

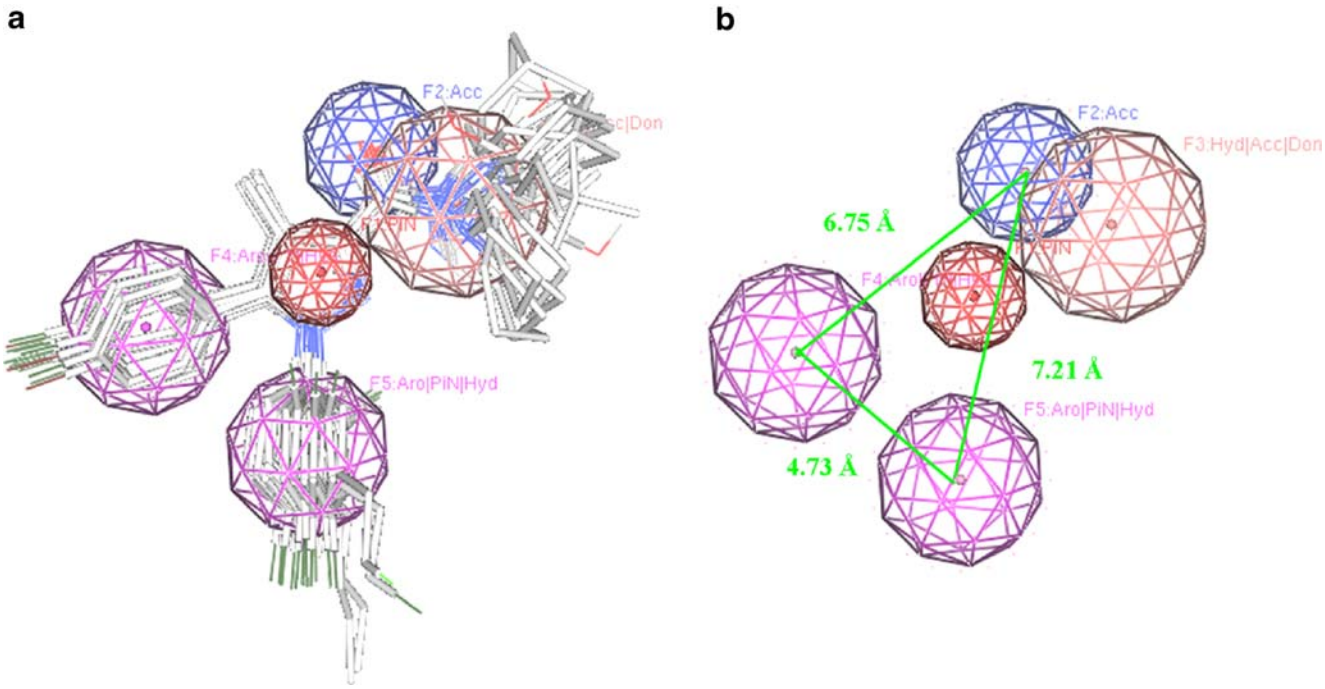

Fig. 3 **(a)** Pharmacophore features shared by compounds **1–24**: Hydrophobic/phenyl centre coloured by purple spheres, hydrophobic centres coloured by red spheres, acceptor functions coloured by blue spheres, hydrophobic nucleus with acceptor function depicted as dark pink spheres. (**b**) Distances among the three key chemical requirements identified by pharmacophore analysis are reported

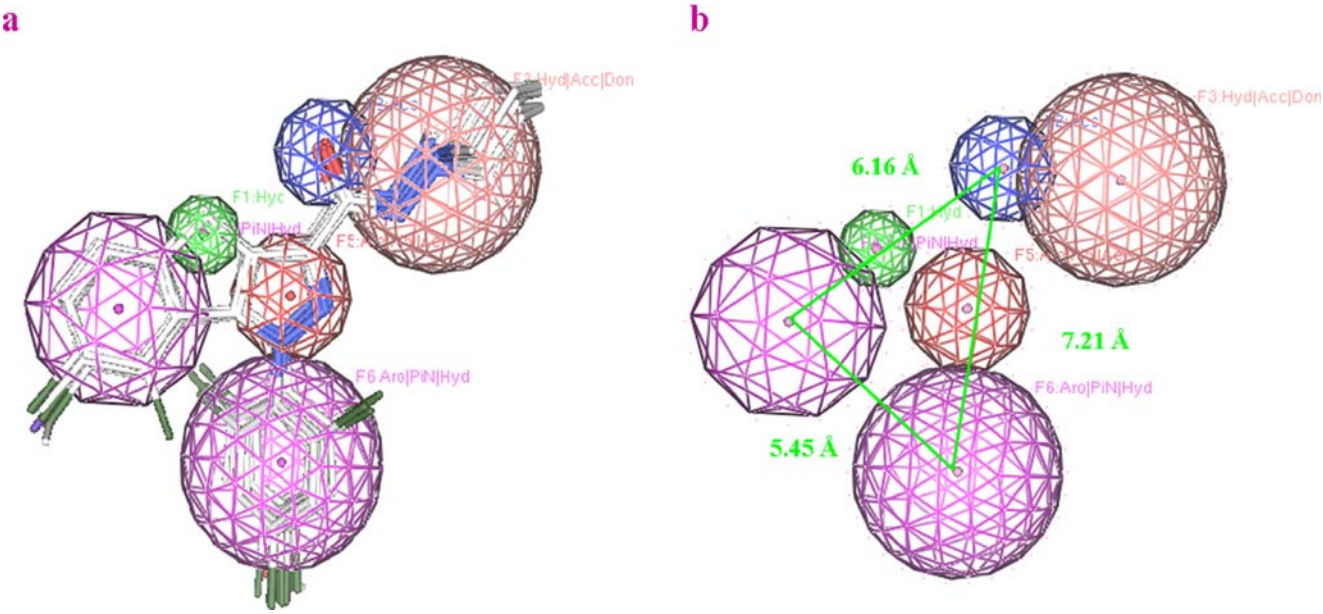

Fig. 4 **(a)** Pharmacophore features shared by compounds **25–39**: Hydrophobic/phenyl centre coloured by purple spheres, hydrophobic centres coloured by red spheres, acceptor functions coloured by blue spheres, hydrophobic nucleus with acceptor function depicted as dark pink spheres, hydrophobic centres are depicted as green spheres. (**b**) Distances among the three key chemical requirements identified by pharmacophore analysis are reported

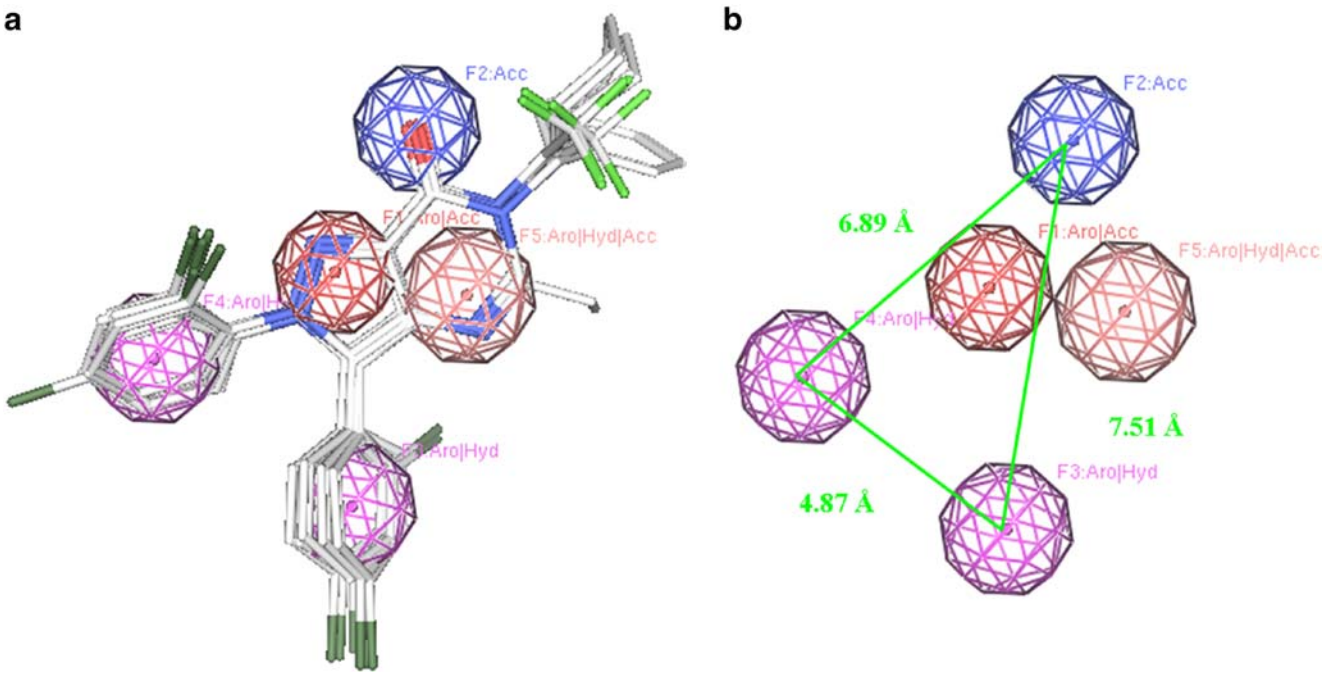

Fig. 5 **(a)** Pharmacophore features shared by compounds **40–47**: Hydrophobic/phenyl centre coloured by purple spheres, hydrophobic centres coloured by red spheres, acceptor functions coloured by blue spheres, hydrophobic centres are depicted as green spheres. (**b**) Distances among the three key chemical requirements identified by pharmacophore analysis are reported

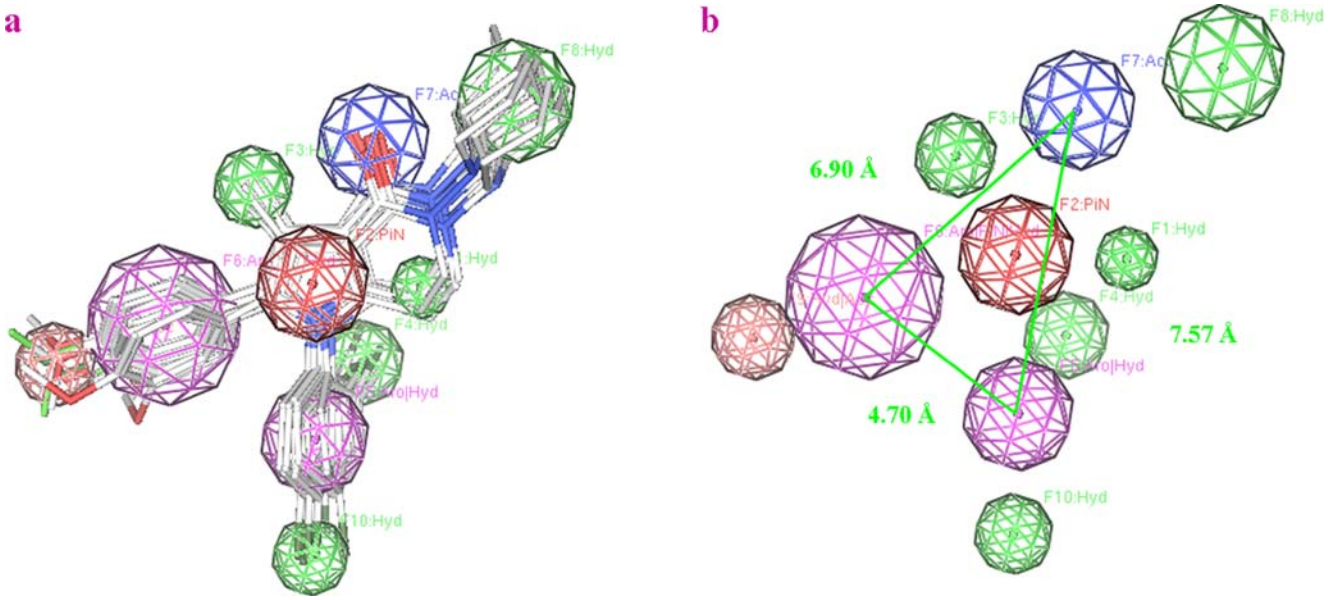

Fig. 6 (a) Pharmacophore features shared by compounds **48–65**: Hydrophobic/phenyl centre coloured by purple spheres, hydrophobic centres coloured by red spheres, acceptor functions coloured by blue spheres, hydrophobic nucleus with acceptor function depicted as dark pink spheres. (**b**) Distances among the three key chemical requirements identified by pharmacophore analysis are reported

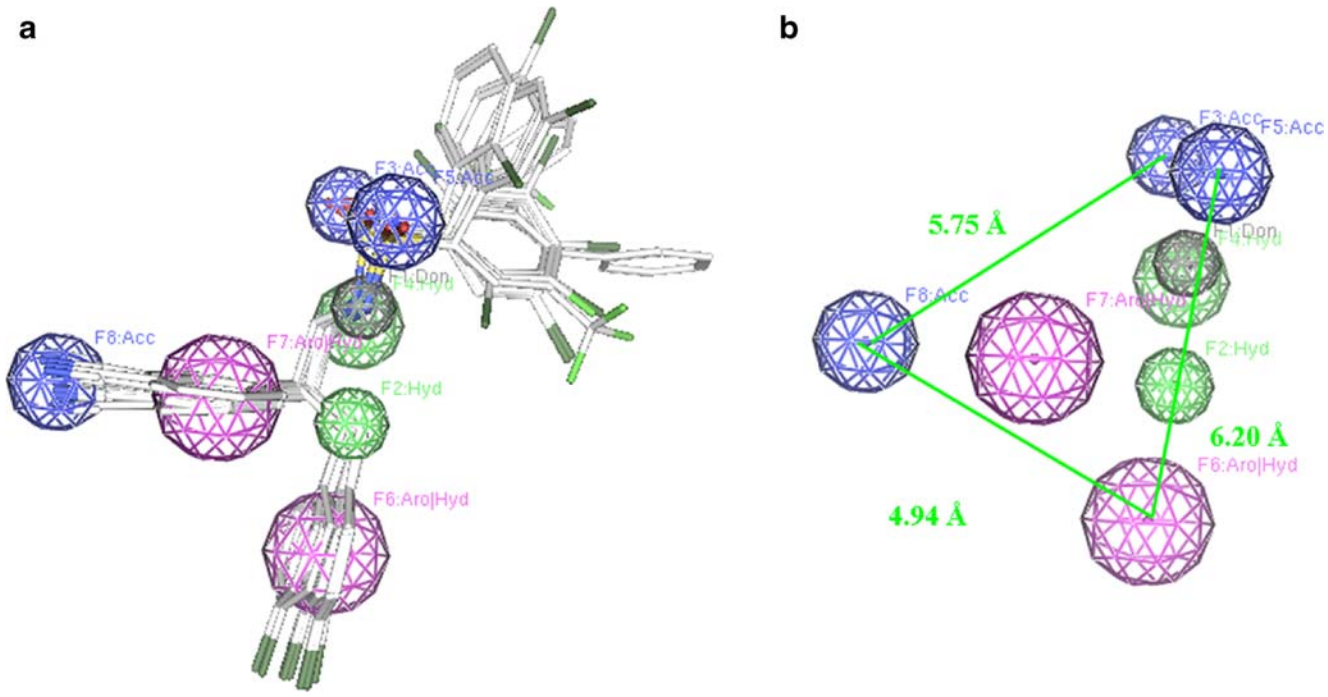

Fig. 7 (a) Pharmacophore features shared by compounds **66–78**: Hydrophobic/phenyl centre coloured by purple spheres, hydrophobic centres coloured by red spheres, acceptor functions coloured by blue spheres, hydrophobic centres are depicted as green spheres. (**b**) Distances among the three key chemical requirements identified by pharmacophore analysis are reported

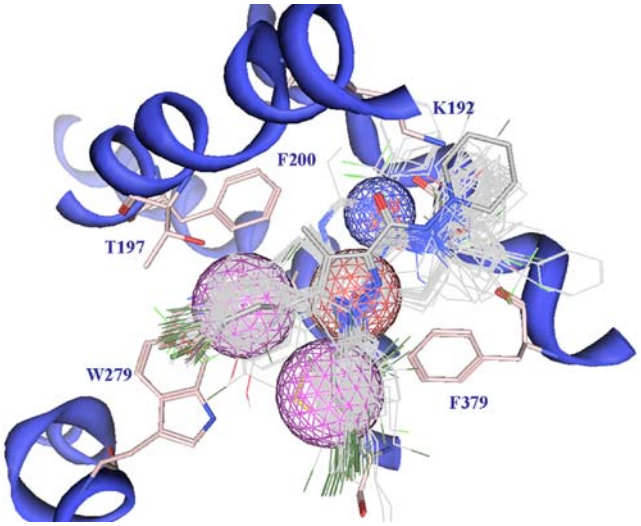

Fig. 8 Compounds **1–78** are aligned into the putative CB_1 receptor binding site. The three key features shared by all of them are reported in coloured spheres. The hydrophobic/aromatic ones are depicted in purple while the acceptor functions are coloured in blue

3D- QSAR analysis

Besides these docking studies, a quantitative evaluation of the structure-activity relationships study inside the class of the CB_1 antagonists has been performed. Compounds **1–78** were manually divided into a training set (**1–6, 8–13, 15–23, 25–31, 33–44, 46–57, 59–61, 63–69, 71–78**) for model generation and into a test set (**7, 14, 24, 32, 45, 58, 62, 70**) for model validation. The analysis was developed using CoMFA steric and electrostatic fields as independent variables and activity (expressed as pKi) as the dependent one.

Table 2 Summary of CoMFA results

No. of compounds	70
Opt. No. components	4
Cross-validated r^2	0.710
Std. error of estimate	0.314
Non cross-validated r^2_{ncv}	0.890
F values	138.773
Steric contribution	0.369
Electrostatic contribution	0.631
Bootstrap r^2	0.931
Std. Error of estimate (bootstrap r2)	0.251
r^2_{pred} [a]	0.893

[a] Correlation coefficient for the test set

CoMFA steric and electrostatic fields effect on the target property can be viewed as 3D coefficient contour plots, thus they could be helpful to identify important regions where any change in these fields may affect the biological activity.

Final CoMFA model was generated using non-cross-validated PLS analysis with the optimum number of components (4) to give an r^2_{ncv} 0.89, Standard Error of Estimate, SEE=0.314, steric contribution=0.369 and electrostatic contribution=0.631. Correlation coefficient for the test set, r^2_{pred} was 0.89.

The results of the CoMFA approach qualitatively points out that the activity of **1–78** is mainly affected by the electrostatic properties of the ligands. The steric and electrostatic fields contour maps of this CoMFA analysis

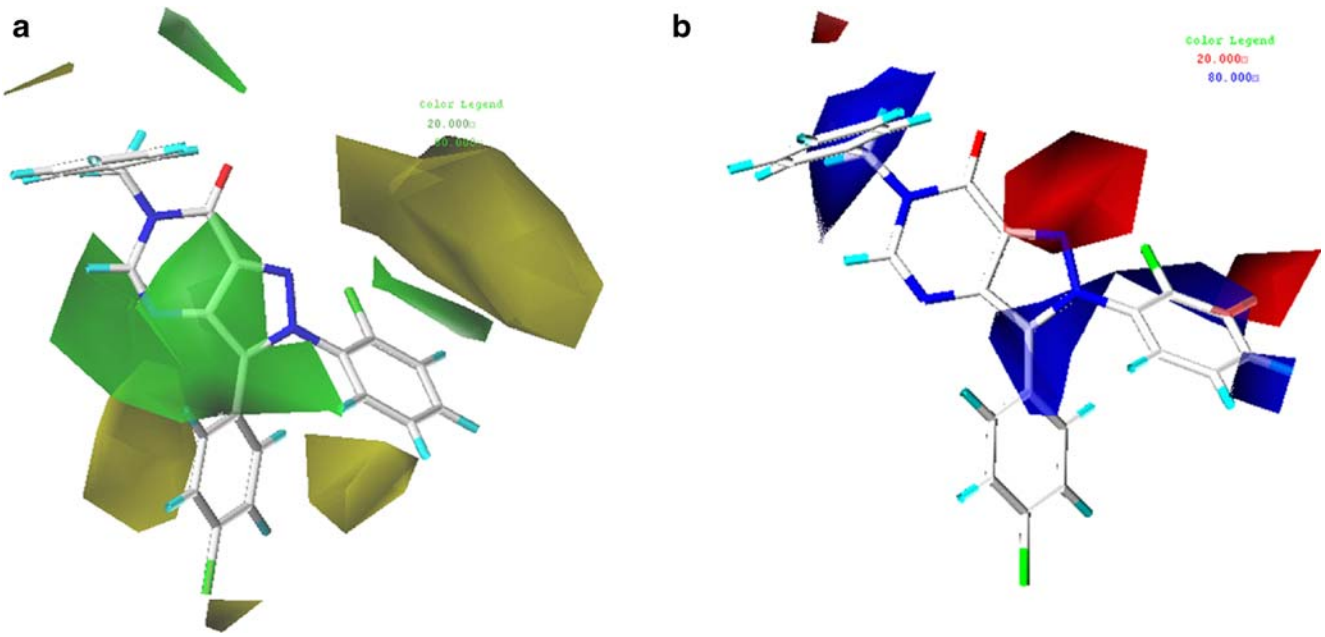

Fig. 9 Steric **(a)** and electrostatic **(b)** CoMFA polyhedra are reported around compound **42** depicted in stick, coloured by atom type

Table 3 Experimental and predicted binding affinities of the test set molecules (**7, 14, 24, 32, 45, 58, 62, 70**)

Compound	pKi exp	pKi pred
7	7.80	7.64
14	6.20	6.42
24	8.30	7.94
32	5.90	5.62
45	8.00	8.23
58	8.50	8.67
62	7.70	7.31
70	7.50	7.89

are plotted in Fig. 9. Taking rimonabant as template for the discussion, the steric contour map shows favourable interaction polyhedra (green region) in the area surrounding bonds 2–3 and 3–4 of the pyrazole ring, thus justifying the positive effects obtained by the substitution of this ring with a bicyclic nucleus such as the pyrazolo-pyrimidinic one (compounds group 3) or the tetrahydropyrrolo-pyridinic one (compounds group 4). On the contrary, the fusion of a ring on bond 4–5 of the pyrazole (compounds group 2) seems to be detrimental for the activity, since the new insertion extends towards a yellow CoMFA region. Moreover, favourable steric interactions are observed in the area corresponding to the *o-m* substituents on the 1-phenyl and in the area corresponding to the *p*-substituent on the 5-phenyl. The same conclusions may be extended to the other compounds of the data-set, aligned together on the basis of their common pharmacophoric features.

As concern the electrostatic maps, all the compounds display those polar moieties involved in hydrogen bonds with Lys192 (described in detail in the Docking poses-Results Session), inside a red region, decoding for a favourable electrostatic interaction.

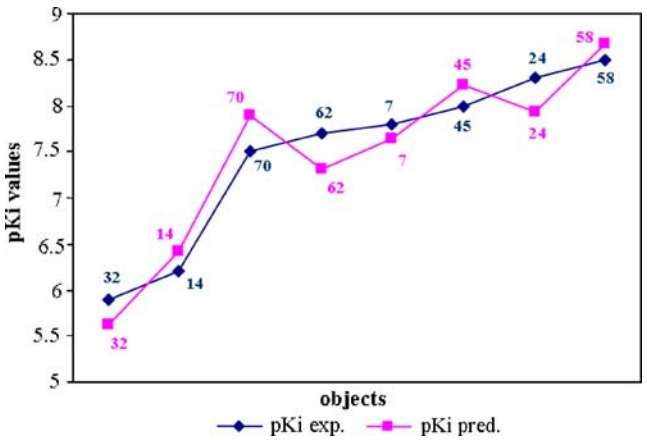

Fig. 10 Plot of experimental and predicted pKi of the test set compounds (**7**, **14**, **24**, **32**, **45**, **58**, **62**, **70**)

Finally, according to our CoMFA study, it seems that the *m*-substituent on the 1-phenyl ring of rimonabant could have polar features, optimally an hydrogen acceptor group, to interact with the counter-part. This consideration is supported by the analysis of CoMFA results for compounds **66**–**78**, which show a cyano function on this position and have the higher biological activity in the data set considered by us.

All statistical parameters supporting CoMFA model are reported in Table 2.

The experimental and predicted binding affinities for test set compounds are reported in Table 3, plot of pKi experimental versus pKi predicted for the test set is reported in Fig. 10.

Conclusions

Our docking analysis puts in evidence the importance of hydrophilic interactions, especially with Lys192 ε amino group, for achieving CB_1 antagonism. In agreement with these results, the CoMFA variable showing the higher value of relevance in the model is the electrostatic component. Moreover, pharmacophore search analysis suggests the existence of some shape and conformational constraints in the compounds of our data set. In order to act as a CB_1 antagonist in fact, the ligand should probably possess a suitable "Y" shape which allows it to fit properly into the three binding pockets (P1, P2, P3) as it is in the case of other GPCRs ligands [17].

The computational strategy here presented will be used as a tool for the screening of virtual libraries with the aim of identifying new CB_1 antagonists.

Acknowledgements Financial support from Italian MIUR (Cofin 2006, prot. 2006030948_002) and Banca Carige S.p.A., Genova, Italy (E.C. grant) are gratefully acknowledged.

References

1. Howlett AC, Barth F, Bonner TI, Cabral G, Casellas P, Devane WA, Felder CC, Herkenham M, Mackie K, Martin BR, Mechoulam R, Pertwee RG (2002) Pharmacol Rev 54:161–202
2. Lambert DM, Fowler CJ (2005) J Med Chem 48:5059–5087
3. de Lago E, Fernández-Ruiz J (2007) CNS Neurol Disord Drug Targets 6:377–387
4. Jagerovic N, Fernandez-Fernandez C, Goya P (2008) Curr Top Med Chem 8:205–230
5. Chen JZ, Han XW, Liu Q, Makriyannis A, Wang J, Xie XQ (2006) J Med Chem 49:625–636
6. Francisco ME, Seltzman HH, Gilliam AF, Mitchell RA, Rider SL, Pertwee RG, Stevenson LA, Thomas BF (2002) J Med Chem 45:2708–2719
7. Mussinu JM, Ruiu S, Mulé AC, Pau A, Carai MAM, Loriga G, Murineddu G, Pinna GA (2003) Bioorg Med Chem 11:251–263
8. Carpino PA, Griffith DA, Sakya S, Dow RL, Black SC, Hadcock JR, Iredale PA, Scott DO, Fichtner MW, Rose CR, Day R, Dibrino J, Butler M, Debartolo DB, Dutcher D, Gautreau D, Lizano JS,

O'Connor RE, Sands MA, Kelly-Sullivan D, Ward KM (2006) Bioorg Med Chem Lett 16:731–736
9. Smith RA, Fathi Z, Brown SE, Choi S, Fan J, Jenkins S, Kluender HC, Konkar A, Lavoie R, Mays R, Natoli J, O'Connor SJ, Ortiz AA, Podlogar B, Taing C, Tomlinson S, Tritto T, Zhang Z (2007) Bioorg Med Chem Lett 17:673–678
10. Armstrong HE, Galka A, Lin LS, Lanza TJ Jr, Jewell JP, Shah SK, Guthikonda R, Truong Q, Chang LL, Quaker G, Colandrea VJ, Tong X, Wang J, Xu S, Fong TM, Shen CP, Lao J, Chen J, Shearman LP, Stribling DS, Rosko K, Strack A, Ha S, Van der Ploeg L, Goulet MT, Hagmann WK (2007) Bioorg Med Chem Lett 17:2184–2187
11. MOE, Chemical Computing Group Inc, Montreal, H3A 2R7 Canada, http://www chemcomp com
12. Fossa P, Menozzi G, Cichero E, Spallarossa A, Ranise A, Mosti L (2008) Eur J Med Chem doi:10.1016/j.ejmech.2008.01.043
13. Cramer RD III, Patterson DE, Bunce JD (1988) J Am Chem Soc 110:5959–5967
14. Sybyl 7 0, Tripos Inc 1699 South Hanley Road, St Louis, MO, USA
15. McAllister SD, Rizvi G, Anavi-Goffer S, Hurst DP, Barnett-Norris J, Lynch DL, Reggio PH, Abood ME (2003) J Med Chem 46:5139–5152
16. Lange JH, Kruse CG (2005) Drug Discov Today 10:693–702
17. Moro S, Bacilieri M, Cacciari B, Bolcato C, Cusan C, Pastorin G, Klotz KN, Spalluto G (2006) Bioorg Med Chem 14:4923–4932